Energy Engineering

Tech Science Press

Doi:10.32604/ee.2025.061590

ARTICLE

Performance Analysis of Solar Porous Media Collector Integrated with Thermal Energy Storage Charged by $CuFe_2O_4$/Water Nanofluids Coil Tubes

Ahmad Mola[1], Sahira H. Ibrahim[1], Nagham Q. Shari[2] and Hasanain A. Abdul Wahhab[3,*]

[1]Mechanical Engineering Department, University of Technology-Iraq, Baghdad, 35050, Iraq
[2]Department of Mechanical Engineering, Wasit University, Kut, 52001, Iraq
[3]Training and Workshop Center, University of Technology-Iraq, Baghdad, 35050, Iraq

*Corresponding Author: Hasanain A. Abdul Wahhab. Email: 20085@uotechnology.edu.iq

Received: 28 November 2024; Accepted: 08 May 2025; Published: 29 May 2025

ABSTRACT: High-efficiency solar energy systems are characterized by their designs, which primarily rely on effective concentration and conversion methods of solar radiation. Evaluation of the performance enhancement of flat plate solar collectors by integration with thermal energy storage could be achieved through simulation of proposed designs. The work aims to analyze a new solar collector integrated with a porous medium and shell and coiled tube heat exchanger. The heat transfer enhancement was investigated by varying the geometrical parameters in shell and helically coiled tubes operating with $CuFe_2O_4$/water with different volume fractions of 0.02%, 0.05%, and 0.1 vol.%. This study presents an experimental and numerical investigation of the performance of the flat plate solar collector integrated with a helical coil heat exchanger using nanofluids. The solar collector has a dimension of 180 cm × 80 cm and works with close-loop systems operated by the thermo siphon method. Two types of helical coil heat exchangers, Coil-A and Coil-B have been investigated. The diameter of the glass porous media was investigated at 2, 5, and 10 mm. The results manifested that the enhancement in the Nusselt number of the nanofluid reached maximum values of 15%, 18%, and 22% for nanofluid ferrofluid with volume concentrations of 0.02%, 0.05%, and 0.1%, respectively, for Coil-A. The maximum values of Nusselt number enhancement were 14%, 17%, and 20% for ferrofluid concentrations of 0.02%, 0.05%, and 0.1 vol.%, respectively, for Coil-B. The results also elucidated that the nanofluid mass flow and heat transfer rates could be noticeably compared to water. Where the increase is 5%, 10%, and 20% for each concentration and diameter of the porous media, it specifies the enormous ranges of operational and geometrical parameters.

KEYWORDS: Nanofluids; porous medium; solar collector; solar water heater; thermal storage materials

1 Introduction

Solar energy (SE) features have led to innovative engineering solutions in building heating, ventilation, and air conditioning (HVAC) systems. SE is environmentally friendly, does not require many people, and does not require constant maintenance. The advancement of science and using different fluids sensitive to heat (nanofluid) in solar collectors with heat exchangers are where heat storage uses a porous medium. This encourages people to use solar energy. ANSYS CFX 16.0 software was used to learn the heat transfer in a pipe and the thermal physics of fluid. A decrease in the heat transfer rate was observed, along with an increase in the mass flow rate [1]. The deliberate heat transfer in both turbo-tube and direct-turbulent heat exchangers is cheated in helical coil (heat exchangers), with two coils of diverse bend relations 0.114 and 0.078, and in cylindrical heat exchangers, respectively in Florida at different rates of 1.89×10^{-4}–6.31×10^{-4} m^3/s as well as for diverse temperatures at the endpoint from 92°C to 149°C. The helix warmth exchangers' total heat

transfer coefficients were much higher than those of the straight tubular heat exchangers. This behavior refers to enhanced heat transfer performance and conserves energy [1,2]. The internal and external heat transfer rates were selected based on the overall heat transfer coefficient and the relationship between the internal heat transfer coefficient and the Reynolds and Prandtl numbers. However, heat transfer for flow between central helical coils was also studied [2].

Double-tube heat exchangers are practical solutions for producing cold and hot industrial air. Therefore, they are displayed using a condenser and a double-pipe evaporator in the air conditioning system, which serves 45 cubic meters of balanced calories with a heat load of 2.24 kW. Evaporator/condenser work produced a promising decrease in compressor work and an increase in the system Coefficient of Performance (COP) [3]. To analyze the performance of solar flat collectors, the inlet and outlet fluid temperatures, thermal efficiency, and combined efficiency are essential parameters. Thermal efficiency is related to the amount of energy transferred from one system component to another without losses. The combined efficiency, on the other hand, considers any energy losses within the system. In addition, different parameters, such as pressure drops and energy consumption, can also be analyzed [4]. The wares of spring-type tabulators situated in an internal pipe of a twin pipe heat exchanger were studied, and the rates of energy transfer, Nusselt number (Nue), and energy waste were studied. Limited ranges of Reynolds numbers ($2500 < Re < 12{,}000$) were chosen, and the range of outer diameters (Ds) of the coils used was 7.2, 9.5, 12, and 13 mm, and turns number (n) of 4, 5, and 6, and turn angle (Ψ) of 0°, 7°, and 10°. Increasing the results of this parameter resulted in a significant augmentation of the energy transfer compared to spring-type (smooth empty tube) [5]. The forced heat transfer procedure was adopted for the calculation in the helical coil heat exchanger, using a nanofluid as the working fluid. The obtained results showed relatively high heat transfer rates with the addition of nanomaterials, where the use of nano copper oxide at weight concentrations (0.3%, 0.6%, 1%, 1.5%, and 2%) showed with varying speeds of the mixing motor at values (500, 1000, and 1500 rpm), the temperatures in the exchanger channels (heating rate) were recorded as 40°C, 45°C, and 50°C. Data were also collected at different flow rates [6].

In counterflow and parallel flow systems, heat transfer in a double tube with triangular baffles was analyzed, and the thermal performance was compared. The results showed an increased heat transfer rate through the collected heat transfer coefficient data [7]. Žandeckis et al. [8] described the augmentation in heat transfer due to using nanofluid in terms of heat transfer rate by noting the collected temperature in the heat exchanger. Also, Lee et al. [9] enhanced the thermal conductivity of fluids by adding nanoparticles. The numerical results of the thermal conductivity of nanofluids with different concentrations of copper nanomaterials are analyzed, the benefits of the additives are assessed, and it is shown that most of the benefits of nanofluids will be dramatic reductions in the operation conditions of the heat exchanger. A mass spectra device was used to catalyze the thermal decomposition of ammonium nitrate of nano-CuO and $CuFe_2O_4$, and a phenomenon, nitrous oxide, formed at an extremely low temperature. Also, two studies of the thermal decomposition phenomenon of ammonium nitrate analyzed by copper oxide/graphene oxide were first recorded according to thermogravimetric mass spectrometry results. The thermal decomposition mechanism of ammonium nitrate with copper oxide/graphene oxide was proposed according to thermogravimetric, differential scanning calorimetric, and thermogravimetric mass spectrometry results [10]. The type of nanoparticles, concentration, and size of nanoparticles are the main features of the enhancement of heat transfer. One of the new studies, an experimental study, is conducted to determine the influence of various concentrations of Al_2O_3 nanoparticles mixed in water as work fluid on the heat transfer features of double pipe heat exchangers for parallel flow and counter flow arrangement. The volume concentrations of Al_2O_3 nanofluid were ranged from 0.001% to 0.01%. The results showed that the overall heat transfer coefficient increases with an increased volume concentration of Al_2O_3 nanoparticles compared to water up to

a volume concentration of 0.008% and then decreases [11]. The type of application and the choice of nanofluid homogenization process are considered the essential features that determine the type, size, load, and shape of nanoparticles used in the solar collector optimization process [12]. Through experiments conducted on a solar flat plate collector using a nanofluid with different nanoparticles, the results confirmed that the heat transfer efficiency of the flat plate was better when using nanofluid at high concentrations, and the results were consistent with what was concluded by [13].

In the experimental investigation by Nasrin and Alim [14], the friction coefficient for laminar flow in the tube containing twisted ribbons was significantly higher than in the conventional tube. Also, the flow behavior of fluids near the tube wall, caused by the twisted ribbon, exhibited higher turbulence intensity than that produced in tubes containing weakly twisted ribbons. The depth and width ratio increased while the heat transfer enhancement increased. Khafaji et al. [15] studied a flat plate solar collector and a heat pipe evacuated tube collector with identical auxiliary components. Both experimental and computational simulations with TRNSYS were conducted to evaluate the system results. The new model used to improve performance contributed to a reduction in the fluid exit temperature from the manifold by 9.6%, and the improvement in the combined heat and power supplied to the load reached 7.6% and 6.9% for the solar flat plate collector system [16].

Akhter et al. [17] presented an experimental investigation of the thermophysical properties of a nanofluid to be used in the medium-temperature solar collector for enhanced thermal energy transport. Thermal conductivity exhibited an increasing trend with rising temperature and an increase in nanoparticle loading [18]. Afolabi et al. [19] experimentally investigated the effect of Fe nanofluid on the performance enhancement of solar water heaters integrated with thermal energy storage systems. The system's efficiency increased from 50.5% to 59.5% with the addition of nanofluid. Also, the water tank temperature increased by 13°C at night. The system's working duration at night has been improved by an average of 5 h with Fe nanofluid. Using the electromagnetic-hydrodynamic approach, Bhatti et al. [20] used a geometric structure composed of a porous material to check third-grade fluid motion through vertical parallel walls. The shooting method was employed to get numerical data for the nonlinear differential equations.

A review of previous work demonstrates that solar heating systems have been improved by developing design models for solar collectors using forced convection principles. Research has also shown increased thermal efficiency by improving the thermal properties of the working fluid, which contributes to raising the system temperature. Therefore, the current work focused on using a nanofluid containing $CuFe_2O_4$ particles due to its superior heat transfer efficiency compared to conventional fluids. The main objective of this study is to conduct an experimental investigation of heat transfer in a solar collector with a porous material lining and using a working fluid containing nanoparticles as a coolant. The solar collector was also integrated with a thermal storage unit to determine the overall system efficiency. The effect of engineering parameters on the heat transfer characteristics of the thermal storage unit was also discussed by changing the design of the helical thermal coil and using $CuFe_2O_4$/water at different volume concentrations to function as a buffer between the spiral coils and the porous medium.

2 Material and Methods

2.1 $CuFe_2O_4$ Nanofluid Characterization and Preparation

Nanofluids are colloidal solutions containing suspended nanoparticles in carrier fluids. In the current work, the sol-gel method was used to prepare $CuFe_2O_4$ nanofluid to analyze the heat transfer in the solar system.

(a) Nano powder preparation

$CuFe_2O_4$ powder was prepared through a chemical process called the sol-gel auto-combustion operation. The ferric nitrate monohydrate Fe (NO_3) $3.9H_2O$ reacted with the high-purity cupric nitrate hydrate Cu (NO_3) $2.6H_2O$, which are considered raw materials. The two materials were gradually mixed with citric acid ($C_6H_8O_7 \times HO$) 2M in a ratio of 1:3 (nitrates:acid). All mixture constituents of these materials were prepared in deionized water and stirred until the result was clear after 2 h.

(b) XRD diffraction

Through the test, a well-defined peak and a sharp were recorded from the sample; all peaks are obtained to the pure cubic phase, and XRD patterns show where 220, 311, 400, 422, 511, and 440 are limits for the main crystal case in $CuFe_2O_4$ spinel ferrite. The generation of a single-phase spinel ferrite structure resulted in an X-ray test, as shown in Fig. 1, Eq. (1) was used for a cubic system for the most intense peak (311) to find the lattice parameter (a):

$$a^2 = (h^2 + k^2 + l^2) \times d^2 \tag{1}$$

h, k, l is the Miller index, and d = the interplanar spacing. For the average grain size (D) and X-ray density (ρx), the average particle size (D_x) is 23.34 nm, calculated using the Debye-Scherrer formula, Eq. (2)

$$D_x = \frac{0.9\lambda}{\beta \cos\theta} \tag{2}$$

Dx = the calculated crystallite size from the broadening of the (311) XRD peak. β = broadening of the diffraction peak, λ = Wavelength of X-ray, and θ = Diffraction angle. Moreover, to calculate the X-ray density (ρx), Eq. (3) was used, which is 5.52 g/cm^3:

$$\rho_x = \left(\frac{8M_w}{N_a \times a^3}\right) \tag{3}$$

M_w = Molecule weight, N_a = Avogadro's number, and a = Lattice constant.

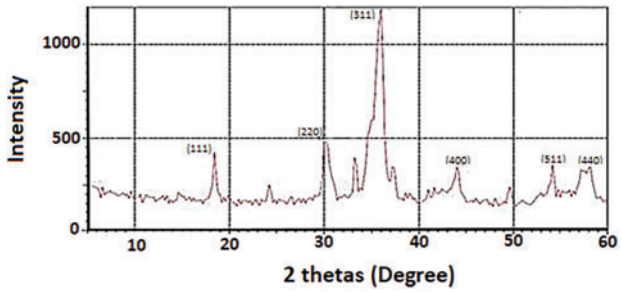

Figure 1: The XRD spectrum of $CuFe_2O_4$ spinel ferrite dust

(c) Preparation of $CuFe_2O_4$ nanofluids

The nanofluid utilized in the experiment was a mixture of $CuFe_2O_4$ oxide and distilled water. The $CuFe_2O_4$ nanofluids were prepared by dispersing $CuFe_2O_4$ nanoparticles in water. The main properties of the materials used in this study are shown in Table 1. After, pre-weighed quantities of nanoparticles were added

to water, and different concentrations of nanofluid were prepared. The volume concentrations of the samples are 0.1, 0.3, 0.5, and 0.7. The concentration is calculated from the equations set in percentage [3,14]:

$$\varphi = \frac{\text{volume of nanoparticles}}{\text{the volume of nanoparticles + volume of water}} \times 100 \tag{4}$$

Or

$$\varphi = \frac{(m/\rho)_{nanopartical}}{(m/\rho)_{nanopartical} + (m/\rho)_{water}} \times 100 \tag{5}$$

Table 1: Main properties of the materials used in the simulations [14]

Substance	$CuFe_2O_4$	Water [14]
Density (kg/m^3)	5400	997
Thermal conductivity ($W/m \cdot K$)	4907	0.607
Specific heat ($J/kg \cdot K$)	3.7	4180
Viscosity ($N \cdot s/m^2$)	700	$8.91 * 10^{-4}$

An important consideration is the uniform homogeneity of the nanoparticles within the distilled water. After preparing the required samples, the thermophysical properties of the nanofluid density, specific heat, viscosity, and thermal conductivity were predicted according to the following set of equations suggested by [11]:

$$\rho_{nf} = (1-\varphi)\,\rho_{bf} + \varphi\rho_p \tag{6}$$

$$Cp_{nf} = (1-\varphi)\,Cp_{bf} + \varphi Cp_p \tag{7}$$

$$\mu_{nf} = \left(\frac{\mu_{bf}}{(1+\varphi)^{2.5}}\right) \tag{8}$$

$$k_{nf} = k_f\left[\frac{2 + k_{pf} + 2\varnothing(k_{pf}-1)}{2 + k_{pf} - \varnothing(k_{pf}-1)}\right] \tag{9}$$

where $k_{pf} = \dfrac{k_p}{k_f}$.

2.2 Experimental Setup

These experiments used two types of heat exchangers, as evidenced in Fig. 2a and b. Coils A and B were manually assembled and connected with the solar collector after the two coils and the shell, as depicted in Table 2. The principles approved by Suryawanshi et al. [21] were adopted accordingly to prepare the design and procedures of the spiral coil heat exchanger in accordance with the standard values.

Fig. 3 represents the experimental setup. The solenoid with the shell was shaped. The pure copper tubes of the helical coil of the heat exchanger were located, and the filter in the middle of the shell was full of porous media. A tank made of galvanization was used as an insulation shell for the heat exchanger, filled with porous media of 86% porosity. This tank was used to save energy, and the other cooled liquid came off

down for up where the step-by-step for controlling the temperature through the experiments. Heat transfer to the inner and outer surfaces of the tank by the forced load is a boundary condition. Different components in the testing system were used, for example, the turbocharger (model: LZM-15, 0.2e2 GPM) to control the flow rate inside the tank. K-type thermocouples were installed in the coil entry and exit points (i.e., T1 and T2). A small fleabag is made by entering and exiting tubes to stop any leakage from the solar collector and coil. The coil's surface has two points (i.e., T3 and T4). Small channels were made carefully, where T1, T2, T3, and T4 were then embedded into the channels and attached to the solar collector and a coil's surface. Two different points of the shell, T5 and T6, are identified to measure the temperature of the water in the shell.

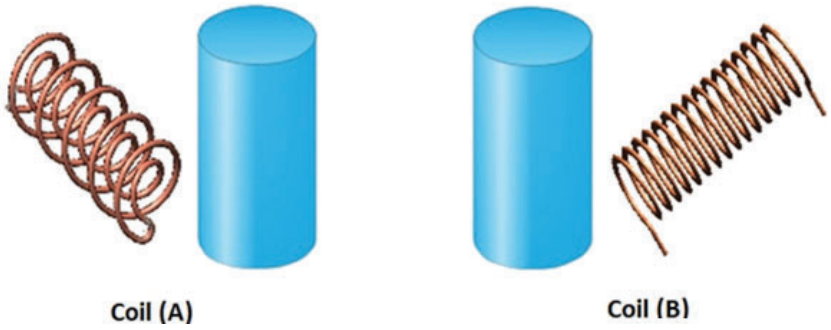

Figure 2: Types of coils

Table 2: Dimensions of coils A, B, and the shell

Parameter	Coil		
	A_{outer}	A_{inside}	B
Outer coil diameter (cm)	18	10	18
Pitch (cm)	8	8	5
Number of turns (N) (turn)	5	5	8
Height (H) (cm)	40	40	40
Pipe diameter (D) (cm)	1.25	1.25	1.25
Pipe length (cm)	440		440
Tank size	L × W × H (30 × 30 × 30)		

A three-day data set for each case has been collected and averaged for the performance analysis. The data were recorded from 7:00 am to 7:00 pm. The method applied by Al-Kayiem and Owolabi [22] was used for the standard measurement and analysis. It was recommended that an equal number of tests should be conducted before and after solar noon. Thus, four data points were recorded: two before solar noon at 11:00 am and 12:00 pm, and the other two after solar noon at 1:00 and 2:00 pm. This was done to eliminate the bias caused by the transient effect. As was recommended, a minimum of 12 data sets should have been obtained, consisting of four inlet temperatures on three different days.

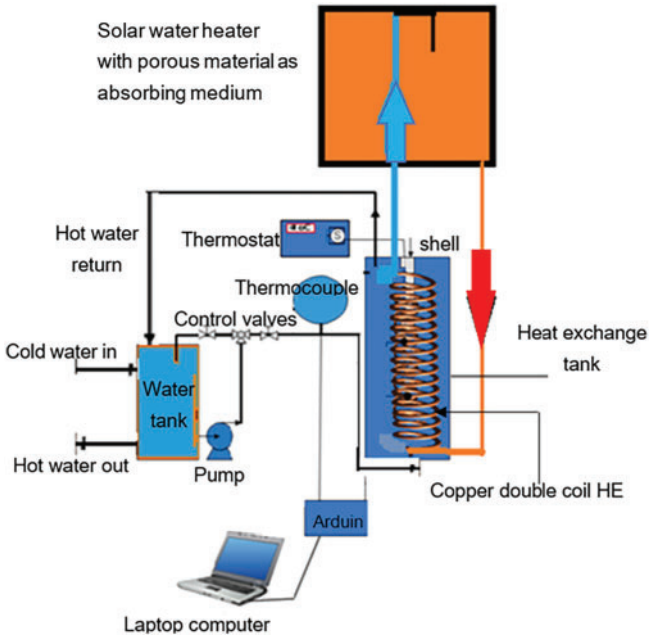

Figure 3: Schematics of the experimental setup

2.3 Model and Data Collection

In the present research, the ANSYS 18.0 FLUENT commercial software achieved a CFD simulation of the hydrothermal process inside the tank and coils. The k-ε model was selected to solve the governing equations with heat transfer under turbulent flow. This simulation is interested in the influence of changing the volume concentration of nanoparticles with water on the heat transfer inside the coil, according to the research objectives.

The investigations were conducted based on the assumptions as follows:

- The physical and thermal properties of the absorber collector surface, thermal energy storage unit, and water with nano additives are independent of the temperature.
- The blend of water with nano additives is continuous and incompressible.
- The nanofluid flow is homogeneous and has characteristics of turbulent flow.
- The heat loss from the bottom of the collector plate is by convection, which depends upon wind speed.
- The changes in the coil shape were assumed to be the exact dimensions of a thermal energy storage unit with complete external insulation.

The improvement in the coil shape in thermal energy storage increased many ideas in the field of heat transfer enhancement. Hence, in this study, two types of coils in the thermal energy storage were simulated. The analysis was conducted by helical coil with varying coil turns and keeping the pipe dimensions constant. All the dimensions were kept the same as in the experimental investigation. Geometry and meshing simulations were performed by the CFD software package of ANSYS 18.0, and the sizing of the grid was performed by command body sizing with 1 mm for the pipe. The detail of nodes and elements of meshing was 1,728,233 and 1,374,139 for Coil-A, and 1,734,534 and 1,394,532 for Coil-B, respectively. When the temperature of the water in the shell starts to heat after a few minutes (often 40 min) for a specific flow rate, the temperature will be variable at the inlet of the coil from the solar collector. Then, the outlet and surface temperatures will be recorded for each case in the research. This research studied the Reynolds number range 5000–10,000,

three-volume concentrations of 0.02%, 0.05%, and 0.1%, two types of coils, and three diameters of Porous Media Glass. As elucidated in the figure, two types of heat exchangers (coils) were used, and all experiments were done on Coil-A and Coil-B, respectively. From which it reaches a stable condition. The set of Eqs. (10) to (13) was used to facilitate the prediction of the Nu values from the side of the nanofluid. The convective heat transfer in the nanofluid, Q_{nf} was predicted using Newton cooling low, Eq. (10).

$$Q_{nf} = \dot{m}_{nf} \times \mathrm{C_{pnf}} \times (T_2 - T_1) \tag{10}$$

The heat flux of each unit area for nanofluid movements in the heat exchanger loop, q_o is premeditated from:

$$q_o = \frac{Q_{nf}}{A_o}, \tag{11}$$

where the contact area is $A_o = \pi \times d_o \times l$

The outside heat transfer coefficient, h_o is calculated from Eq. (10).

$$h_{in} = \frac{q_o}{(T_b - T_s)} \tag{12}$$

$$\mathrm{Nu_h} = \frac{h_{in} * \mathrm{D_{in}}}{k_{nf}} \tag{13}$$

The porosity, ε of the porous medium is a parameter for each particle with a constant diameter of 11.7 mm. The void of a porous medium is given by [14].

$$\varepsilon = \frac{v_{total} - v_{soilds}}{v_{total}} \tag{14}$$

The permeability, k, depends on the porosity of the glass sphere diameter, which has been selected as 2, 5, and 10 mm, and estimated by Eq. (15).

$$\mathrm{k} = \frac{d_S^2 \varepsilon^3}{150(1-\varepsilon)^2} \tag{15}$$

The penetrability of the glass spheres originated to be $2.0529 * 10^{-7}$ $\mathrm{m^2}$.

An important property of the porous medium is the effective thermal conductivity, k_m.

$$k_m = \varepsilon k_f + (1-\varepsilon)\, k_s, \tag{16}$$

where k_f, operated at the normal working temperature of 60°C, is 0.02865, and k_s is taken from [9]. The prediction values made by Eq. (4) were acceptable only if $k_f \approx k_s$, i.e., the conductivity ratio, $\lambda = k_f / k_s \cong 1$.

Based on a two-dimensional heat transfer model, where the conductivity ratio is less than unity, λ = 0.1155, for a better choice to use Krupiczka's correlation (Prasad 1989). The correlation is given by Eq. (17).

$$k_m = k_f * \lambda^{-n} \tag{17}$$

where:

$$n = 0.28 - 0.757 log10\varepsilon + 0.057 log10\lambda \tag{18}$$

2.4 Uncertainty Analysis

Generally, the combined experimental uncertainty consisted of systematic and random uncertainties to determine the solar system's performance. The systematic uncertainties were the errors from the measuring instruments caused by data recording errors and calibration errors. While the random uncertainty is the data scatter uncertainty caused by the fluctuation of the calculated parameter.

The systematic uncertainty (δ) quantifies the expected accuracy, but it does not guarantee accuracy. The discrepancy between the measured value and the true value of the quantity, Eq. (19). A more realistic method is to use the root-sum-of-squares method, that is, by taking the square root of the sum of the individual errors [22].

$$measured\ value = true\ value \pm error \tag{19}$$

$$\delta = \sqrt{(\delta_{sensor})^2 + (\delta_{instrument})^2} \tag{20}$$

$$Min.\&Max.Uncer.\,(\delta\%) = 100 \times \left(\frac{\delta}{Min.\&Max.Reading}\right) \tag{21}$$

The random uncertainty (γ) in the calculations was needed to know the repeatability and reproducibility of the results.

$$\gamma(\%) = \left(\frac{S_E}{\overline{X}}\right) \times 100 \tag{22}$$

$$S_E = \frac{\sigma}{\sqrt{n}} \tag{23}$$

where S_E is the standard error, X is the mean of the collected data, σ is the standard deviation, and n is the repeatable readings of heat transfer coefficient, Nusselt number, and efficiency factor. The equation below shows the combined uncertainty (ω_t).

$$\omega_t = \sqrt{\delta^2 + \gamma^2} \tag{24}$$

Table 3 shows the uncertainty percentage error of the experimental data.

Table 3: The uncertainty percentage error of the experimental data

The systematic uncertainty			
Parameter	**Min. value**	**Max. value**	**δ (%)**
Water flow rate	15.6 SLPM	32.5 SLPM	±0.44–±0.28%
Temperature	31°C	73°C	±0.21–±0.13%
The random uncertainty			
Parameter		**value**	**γ (%)**
Heat transfer coefficient		68–132	±1.67%
Nusselt number		41–153	±1.12%
Efficiency factor		0.91–0.98	±0.06%
The combined uncertainty (ω_t)			±2.035%

3 Results and Discussion

In microstructure, the ferrites powder calcined at 500°C was investigated, as seen in Fig. 4. The SEM picture of $CuFe_2O_4$ powder has high pores. The fresh catalyst has a broad pore size distribution of 5–50 nm with an average pore size of 13–14 nm) outfit structure, where the powders look like ash, and the pores are clear in a sample. It was found that the particles are irregular in shape, and the mean Nanoparticle size is 50 nm.

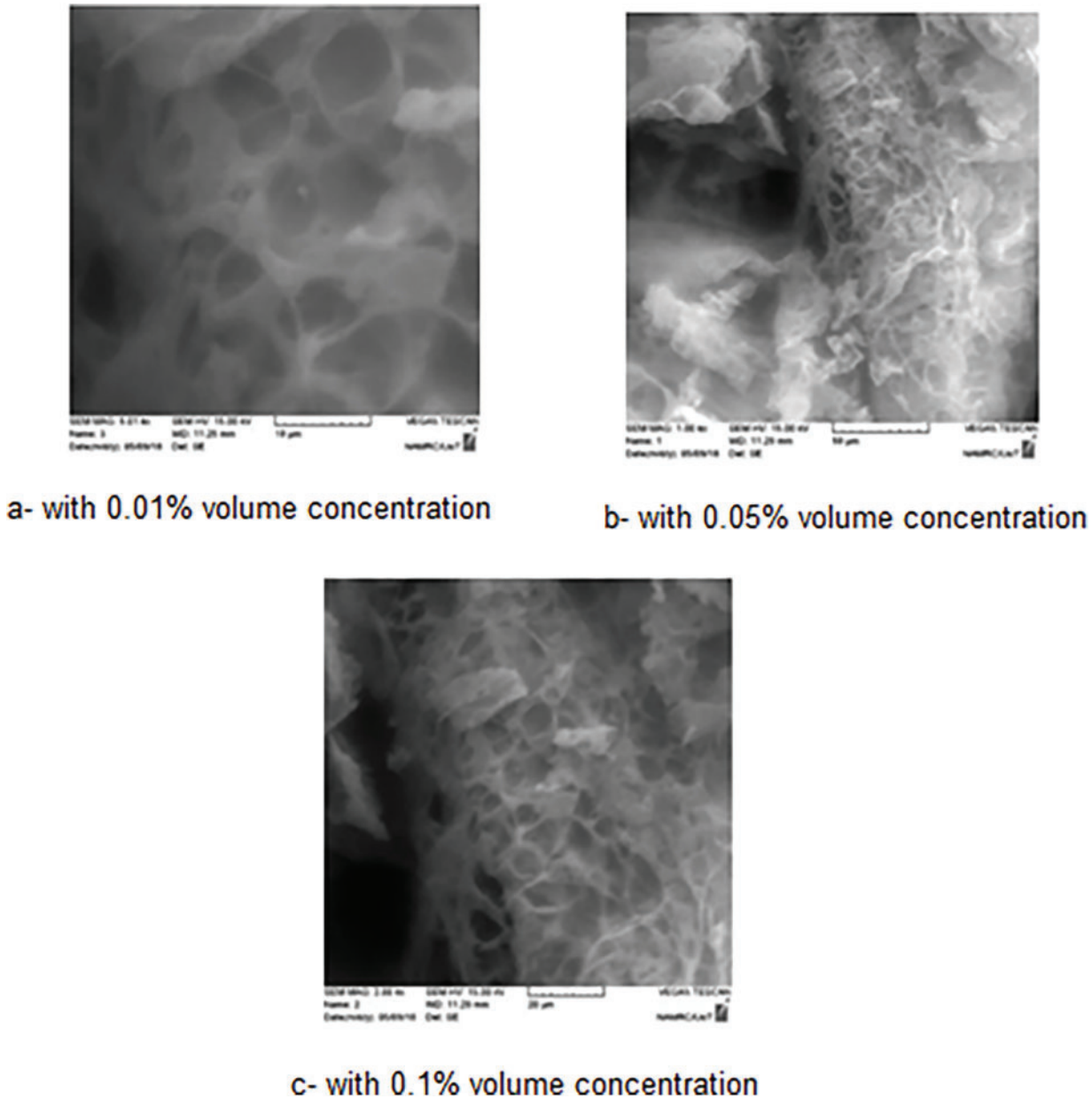

Figure 4: SEM picture of $CuFe_2O_4$ spinel ferrite dust

Nanofluids are suspended metallic or non-metallic nano powders from 1 to 100 nm in base fluid water and are synthesized to provide considerable preferences over conventional heat transfer fluids. Heat transfer

characteristics can be increased by improving the thermos physical properties of nanofluid as the results were elucidated in relation to the mass flow rate and the heat transfer for the nano-additives. In an attempt to investigate the correlation of the performance of the nano absorption unit using solar energy, this heated water was fed into a shell. A similar performance was obtained using a 100 kW coil, as represented in Fig. 5. The time required to obtain 90°C temperature at the helical coil, using 250, 200, 150, and 100 kW, was shortened to 34, 41, 53, and 59 min, respectively. Heating coils are plotted against the time required using water heated by solar energy to heat the regulator. Considering the simple assumption made in the analytical approach, it is practicable that the suggested optimum pitch could be employed in designing a coil with a flat plate solar tubular collector for $CuFe_2O_4$ and water heating in the Baghdad area. The investigation repeated on a flat solar day revealed that the intensity of solar radiation at the same time was only 60% to 80% of the usual intensity. Also, the figure recorded the variation of temperature distribution of coil (A) at different volume concentrations of $CuFe_2O_4$ blended with water 0%, 0.02%, 0.05%, and 0.1%. In general, the temperature distributions of the coil increase gradually in the flow direction. The absorber coil temperature of the thermal energy storage unit with enhanced water by nanomaterials at 0.1% concentration is higher than the other cases. The enhanced thermal properties of the fluid inside the coil lead to an increase in the heat transmitted from and to the storage unit, and the fluid finally leads to an increase in the absorber coil temperature.

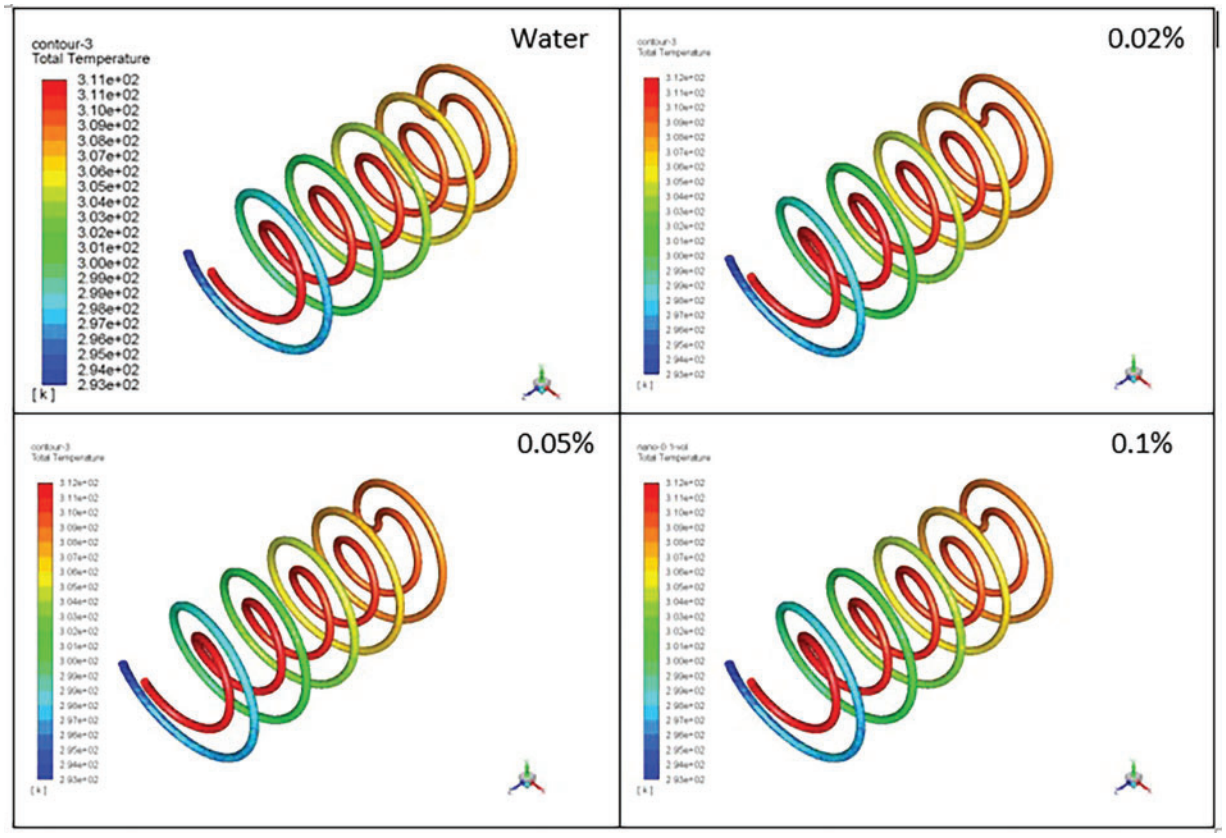

Figure 5: Temperature contour along the test section coil A at volume concentrations of 0%, 0.02%, 0.05%, and 0.1% with Porous Media glass 2 mm

The heat exchanger efficiency is affected by applying a porous medium in the tank, and the heat exchanger efficiency factor changes with the Nu number. The test included two coil shapes to represent the most useful energy gain that would result if the tank absorbing surface was at the local fluid temperature. Fig. 6 is plotted to investigate the effects of the convection-conduction parameter on the heat exchanger efficiency factor. It depicts that the heat exchanger efficiency factor increases with decreasing the loss coefficient (UL), and the results show that the heat exchanger efficiency factor for coil A is higher than for coil B. Variations in the heat exchanger efficiency factor are based on variations in the coil geometry and increased surface area of the coil. Double coils with different sizes in model A tend to absorb and scatter heat with high performance. This trend agreed with the previous publication by Tlau and Ontela [23]. The heat exchanger efficiency factor for the case with coil-A increases with the volume concentration (0%, 0.02%, 0.05%, 0.1%) and with the porous media glass 2 mm due to the increased Nu number. Also, the increase in volume concentration can cause an increase demonstrated as the effectiveness of a conventional heat exchanger, which is defined as the heat exchanger factor, as illustrated in Fig. 7.

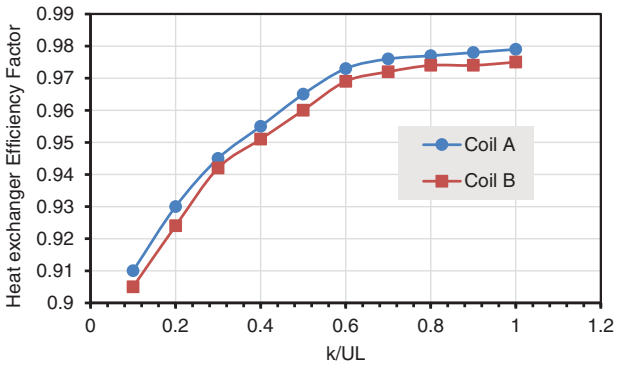

Figure 6: Heat exchanger efficiency factor versus k/UL for coil-A and coil-B with Porous Media glass 2 mm

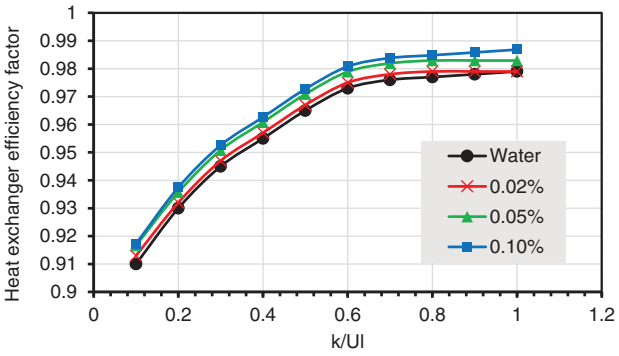

Figure 7: Heat exchanger efficiency factor versus k/UL for coil A at volume concentration (0%, 0.02%, 0.05%, 0.1%) with Porous Media glass 2 mm

Fig. 8 compares the experimental and numerical results of the heat exchanger efficiency factor and k/UL with different conditions of water flow alone and nanofluid at 0.1% volume concentration. The different percentages of the heat exchanger efficiency factor were 7.2% and 8.9% for water and nanofluid, respectively. A difference in the heat exchanger efficiency factor was observed in the experimental data and numerical data around 8%. The reason for this is that the numerical heat transfer has ideal characteristics compared to

the experimental test, such as improving the thermal efficiency by adding nanoparticles to water. In addition, it improves the heat absorption properties compared to water.

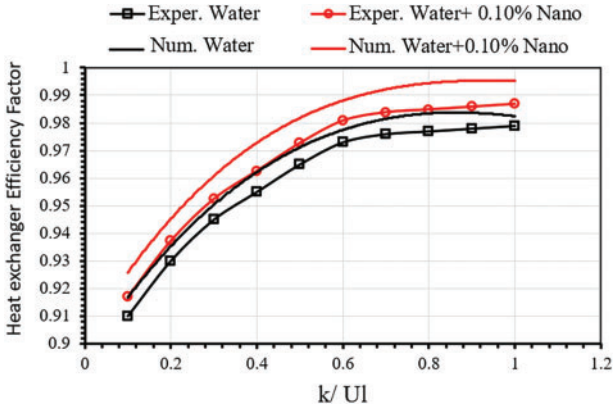

Figure 8: Comparison of numerical and experimental results of heat exchanger efficiency factor vs. k/UL for coil A at water alone and water + nano 0.1% volume concentration

Fig. 9 evidences the average Nusselt number variation with Reynolds number for coil A and coil B at volume concentration (0.1%) of nanoparticle for used porous media 2 mm, which is increased from 21.2 to 52.5 as the Reynolds number increased from 4500 to 12,500. This variation was compared with the previous empirical correlation of Dittus-Boelter for heat transfer inside the smooth tube equation. As depicted in this figure, there is a good agreement, and the maximum deviation is 14%. The extent of the improvement in heat transfer through coil A compared to coil B is due to the more homogeneous mixing of the working fluids due to the increase in centrifugal force by increasing the number of turns of the coil, which causes the growth of the secondary flow. This procedure is the main reason responsible for the lower high friction pressure in the spiral tube than in the coil with fewer turns or the straight tube within the same dimensions.

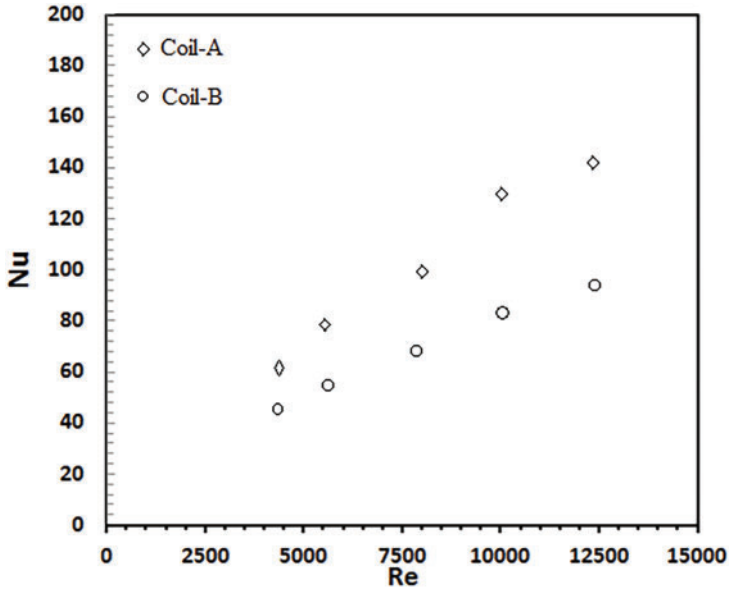

Figure 9: Comparison of average Nusselt numbers for coils A and B at a volume concentration of 0.1% for a Reynolds number range of 4500–12,500 with a glass porous medium of 2 mm

On the other hand, several practical equations were used to calculate the Nu number, and the pressure dropped inside the coiled pipe. A validation between numerical and experimental results for the same Reynolds number showed that the predicted data and prediction accuracy depended on the fluid flow conditions. Therefore, the usefulness of these equations for designing helical coil heat exchangers needs more experiments under different conditions. On the other hand, the error between the predicted value and the experimental value was around ±5.8%. The empirical correlation for different Nusselt numbers and Reynolds numbers was based on volume concentrations, which was given in Eq. (13).

Using the nanofluid leads to an enhancement of the heat exchanger efficiency factor. This implies that the heat losses decrease in the nanofluid flow in comparison to the base fluid. Furthermore, the greater concentration has lower heat losses. Increasing the flow rate increases the Re value, leading to higher Nusselt number values within the fully turbulent tested range of Re in all investigated nano concentrations. This phenomenon can be elucidated by perusing the governing energy equation. The correlation was compared to data from previous studies in Fig. 10.

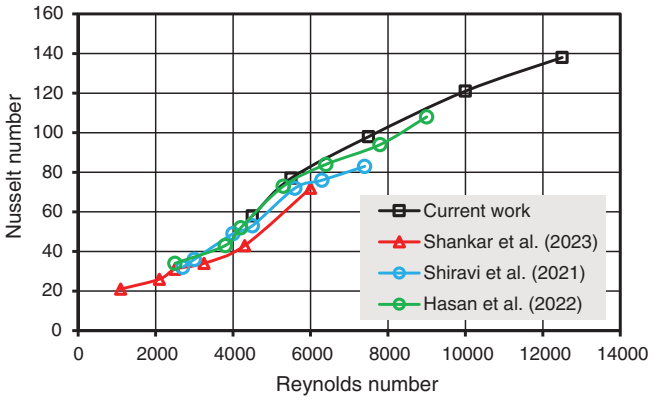

Figure 10: Comparison of current results with previous studies [24–26]

Fig. 10 presents multiple data sets from different studies that are compared, including the current study, as well as references from various researchers. As turbulent flow inside the coil increases (Reynolds number between 4500 to 12,500), the Nusselt number generally increases across all data sets [24–26]. This aligns with the increasing pressure drop in the coiled pipe with high fluid flow. The current study shows a consistently higher Nusselt number than others, especially at higher values of Re number.

There is no doubt that solar water heating reduces the reliance on fossil fuels, which are a major source of greenhouse gas emissions. Using advanced and highly performing SWH would help to mitigate climate change. Since SWHs operate without fossil fuel combustion, they contribute to cleaner air quality. In addition to the environmental issues, utilizing solar power as a renewable energy source would significantly reduce energy bills over time, leading to a more efficient use of resources without compromising environmental standards.

However, there is still a limitation in the adoption of SWH, where potential environmental drawbacks, such as the energy and materials used in the manufacturing and disposal of solar collectors. In the long-term usage of the SWH system, the issue of disposal and recycling is outweighed by the environmental benefits.

Summing up, the advanced and efficient SWH contributes positively to environmental Sustainability by reducing emissions and supporting the transition to renewable energy.

4 Conclusions

This study experimentally and numerically investigates a flat plate solar collector integrated with thermal storage with a view to improving performance characteristics. A $CuFe_2O_4$ nano-in-water nanofluid was used as a heat transfer fluid. The idea in this design focused on increasing the area exposed to solar radiation to improve the absorption capacities by glass porous medium in 2, 5, and 10 mm diameter tubes. The study includes two models of helical coil heat exchangers, coil A and coil B. Three concentrations of nanofluid of 0.02%, 0.05%, and 0.1% were used to assess the system performance. The following conclusions are drawn:

- The enhancement in the Nusselt number of the nanofluid reached values of 14%–15%, 17%–18%, and 20%–22% for nano volume concentrations of 0.02%, 0.05%, and 0.1%, respectively, compared to water.
- The optimal volume concentration of $CuFe_2O_4$ is 0.1 vol.%, and the flow rate is 32.5 L/min. At 0.1 vol.%, the pressure drop may increase, giving a higher heat exchanger efficiency factor for Coil A.

CFD analysis is conducted by two coil designs and different concentrations of nanomaterials. Future works are required to be conducted for further refinements of helical heat exchangers by simulation analysis and optimization by changing the curvature ratio and varying the pitch of the helical coil under a wider range of Re to cover laminar, transition, and turbulent flow. In addition, the design of the experimental model could be investigated with various configurations of the porous medium.

Acknowledgement: The authors acknowledge the University of Technology-Iraq, Baghdad, for the technical support to conduct the research by allowing the use of the Center for Renewable and Sustainable Energy Facilities.

Funding Statement: There is no funding for this research.

Author Contributions: The authors confirm their contribution to the paper as follows: study conception and design: Ahmad Mola, Hasanain A. Abdul Wahhab, Sahira H. Ibrahim; data collection: Sahira H. Ibrahim, Nagham Q. Shari; analysis and interpretation of results: Hasanain A. Abdul Wahhab, Nagham Q. Shari; draft manuscript preparation: Ahmad Mola, Hasanain A. Abdul Wahhab. All authors reviewed the results and approved the final version of the manuscript.

Availability of Data and Materials: The datasets are available to the corresponding author upon reasonable request.

Ethics Approval: Not applicable.

Conflicts of Interest: The authors declare no conflicts of interest to report regarding the present study.

Nomenclature

Dx	The average particle size (nm)
h, k, l	The Miler index (-)
d	The inter planer spacing (mm)
ρx	The X-ray density
λ	Wavelength of X-ray
β	Broadening of the diffraction peak (-)
θ	Diffraction angle (deg)
φ	The volume concentration (ppm)
Mw	Molecule weight (mole/m^3)
Na	Avogadro's number (-)
a	Lattice constant (-)
ε	The void of a porous medium (-)

k	Permeability Measurement
km	Design of the Effective Thermal Conductivity (W/m · K)
T1 to T6	Locations of thermocouples for temperature measurements (K)

References

1. Ibrahim SH, Abdul Wahhab HA. Influence of twisted tape inserts with perforation on heat transfer and pressure drop inside the circular tube: numerical and experimental investigation. In: Proceedings of ICPER 2020, Lecture Notes in Mechanical Engineering. Springer; 2023. p. 281–93. doi:10.1007/978-981-19-1939-8_24.
2. Du S, Ren Q, He YL. Optical and radiative properties analysis and optimization study of the gradually varied volumetric solar receiver. Appl Energy. 2017;207:27–35. doi:10.1016/j.apenergy.2017.05.165.
3. Bahrehmand S, Abbassi A. Heat transfer and performance analysis of nanofluid flow in helically coiled tube heat exchangers Chem. Eng Res Design. 2016;109(1–2):628–37. doi:10.1016/j.cherd.2016.03.022.
4. Singh I, Singh D, Singh M. Thermal modeling and performance evaluation of photovoltaic thermal (PV/T) systems: a parametric study Inter. J Green Energy. 2019;16(6):483–9. doi:10.1080/15435075.2019.1584103.
5. Manish S, Devendra Y, Mayank B, Gurjeet S. Enhancing the thermal performance of a double pipe heat exchanger in turbulent flow conditions. Int J Thermodyn. 2022;25(2):099–111. doi:10.5541/ijot.1059520.
6. Neuberger P, Adamovsktfytf R, Šeďová M. Temperatures and heat flow in a soil enclosing a slinky horizontal heat exchanger. Energies. 2014;7(2):972–87. doi:10.3390/en7020972.
7. Kharat R, Bhardwaj N, Jha RS. Development of heat transfer coefficient correlation for concentric helical coil heat exchanger. Int J Ther Scie. 2009;48(12):2300–8. doi:10.1016/j.ijthermalsci.2009.04.008.
8. Žandeckis A, Kļaviņa K, Dzikēvičs M, Kirsanovs V, Žogla G. Solutions for energy efficient and sustainable heating of ventilation air: a review. J Eng Scie Tech Rev. 2015;8(3):98–111. doi:10.25103/jestr.083.14.
9. Lee S, Choi SUS, Li S, Eastman JA. Measuring thermal con nanoparticles. J Heat Tran. 1999;121(2):280–9.
10. Tsai TH, Chein R. Performance analysis of nano-fluid-cooled microchannel heat sinks. Int J Heat Fluid Flow. 2007;28(5):1013–26. doi:10.1016/j.ijheatfluidflow.2007.01.007.
11. Shamshirgaran SR, Al-Kayiem HH, Sharma KV, Ghasemi M. State of the art of techno-economics of nanofluid-laden flat-plate solar collectors for sustainable accomplishment. Sustainability. 2020;12(21):9119. doi:10.3390/su12219119.
12. Lee J, Mudawar I. Assessment of the effectiveness of nanofluids for single-phase and two-phase heat transfer in micro-channels. Int J Heat Mass Tran. 2007;50(3–4):452–63. doi:10.1016/j.ijheatmasstransfer.2006.08.001.
13. Shamshirgaran SR, Assadi MK, Sharma KV. Application of nanomaterials in solar thermal energy storage. Heat Mass Trans. 2018;50(6):1555–77. doi:10.1007/s00231-017-2259-1.
14. Nasrin R, Alim MA. Heat transfer by nanofluid with different nanoparticles in a solar collector. Heat Trans—Asian Res. 2014;43(1):61–79. doi:10.1002/htj.2106-1.
15. Khafaji HQA, Abdul Wahhab HA, Alsaedi SS, Al-Maliki WAK, Alobaid F, Epple B. Thermal performance evaluation of a tubular heat exchanger fitted with combined basket-twisted tape inserts. Appl Sci. 2022;12(10):4807. doi:10.3390/app12104807.
16. Ajel MG, Gedik E, Abdul Wahhab HA, Shallal BA. Performance analysis of an open-flow photovoltaic/thermal (PV/T) solar collector using a different fins shapes. Sustainability. 2023;15(5):3877. doi:10.3390/su15053877.
17. Akhter J, Gilani SI, Al-Kayiem HH, Ali M, Masood F. Experimental evaluation of thermophysical properties of oil-based titania nanofluids for medium temperature solar collectors. Mate Sci Eng Tech. 2020;21(6):792–802. doi:10.1002/mawe.201900244.
18. Akhter J, Gilani SI, Al-Kayiem HH, Ali M, Masood F. Characterization and stability analysis of oil-based copper oxide nanofluids for medium temperature solar collectors. Mater Sci Eng Tech. 2019;50(3):311–9. doi:10.1002/mawe.201800220.
19. Afolabi LO, Al-Kayiem HH, Baheta AT. Performance investigation on a thermal energy storage integrated solar collector system using nanofluid. Int J Energy Res. 2016;41(6):3657. doi:10.1002/er.3657.

20. Bhatti MM, Abbas MA, Muhammad S. Chapter 9-Optimizing fluid flow efficiency: third-grade hybrid nanofluid flow with electro-magneto-hydrodynamics in confined vertical spaces. In: Rashidi MM, Zinatloo-Ajabshir S, editors. Micro and nano technologies, Nanofluids preparation, applications and simulation methods micro and nano technologies. Elsevier; 2024. p. 243–75. doi: 10.1016/B978-0-443-13625-2.00012-7.
21. Suryawanshi VV, Ghodake N, Patil O, Lomate S, Nerkar SG. Design and analysis of helical coil heat exchanger. Int J Eng Rese Mech Civ Eng. 2021;6(8):28–33.
22. Al-Kayiem HH, Owolabi AL. Enhancement techniques for solar energy technologies. In: Picón-Núñez M, editor. Solar collectors: applications and performance. New York, NY, USA: NOVA Science Publisher; 2018.
23. Tlau L, Ontela S. Entropy analysis of hybrid nanofluid flow in a porous medium with variable permeability considering isothermal/isoflux conditions. Chin J Phys. 2022;80:239–52. doi:10.1016/j.cjph.2022.10.001.
24. Shankar N, Perumalsamy SP, Chandran M. Heat transfer enhancement in a helically epically coiled convergent and divergent tube heat exchanger with Al_2O_3 nanofluid. Therm Sci. 2023;27(6A):4707–18. doi:10.2298/TSCI221205140S.
25. Shiravi AH, Shafiee M, Firoozzadeh M, Bostani H, Bozorgmehrian M. Experimental study on convective heat transfer and entropy generation of carbon black nanofluid turbulent flow in a helical coiled heat exchanger. J Therm Anal Calorim. 2021;145(2):597–607. doi:10.1007/s10973-020-09729-1.
26. Hasan MJ, Ahmed SF, Bhuiyan AA. Geometrical and coil revolution effects on the performance enhancement of a helical heat exchanger using nanofluids. Case Stud Therm Eng. 2022;35:102106. doi:10.1016/j.csite.2022.102106.